

## **Manufacturability of A20X printed lattice heat sinks**

CHOUHAN, Ganesh and BIDARE, Prveen

Available from Sheffield Hallam University Research Archive (SHURA) at:

<https://shura.shu.ac.uk/34626/>

---

This document is the Published Version [VoR]

### **Citation:**

CHOUHAN, Ganesh and BIDARE, Prveen (2024). Manufacturability of A20X printed lattice heat sinks. Progress in Additive Manufacturing. [Article]

---

### **Copyright and re-use policy**

See <http://shura.shu.ac.uk/information.html>



# Manufacturability of A20X printed lattice heat sinks

Ganesh Chouhan<sup>1</sup> · Prveen Bidare<sup>2,3</sup>

Received: 21 August 2024 / Accepted: 5 December 2024  
© The Author(s) 2024

## Abstract

Laser powder bed fusion (LPBF) is a well-established technique for manufacturing compact and intricate lattice structures; however, surface roughness on curved surfaces remains a notable limitation. Triple periodic minimal surface lattices are beneficial for their lightweight, high-strength components and increased surface area for heat transfer, making them highly desirable in aerospace applications. This study designs five TPMS lattice-based heat sinks (Gyroid, Diamond, Lidinoid, Schwarz P, and Split P) utilizing two unit cell sizes (5 mm and 10 mm), with a consistent thickness of 1 mm and a base thickness of 2 mm, all within a specified volume of  $15 \times 15 \times 15 \text{ mm}^3$ . Additionally, two cylindrical designs featuring varying periodicity for the gyroid and diamond lattices have been developed, utilizing unit cell sizes of 5 mm and 10 mm. The laser powder bed fusion technique was employed to fabricate A20x aluminium-based heat sinks, achieving excellent surface quality. Surface texture characterization of metal heat sinks was conducted using surface topography analysis with an optical profilometer and microstructural examination via scanning electron microscopy. Additionally, the relative density of the LPBF-printed heat sinks was measured to be over 99.5%.

**Keywords** Heat sink · Lattice structure · Triply periodic minimal surface · Manufacturability · Aluminium A20X

## 1 Introduction

Thermal analysis is important in a variety of engineering fields, especially in the examination of electronic devices. Compact electronic devices are indeed the current trend, and this will result in a large increase in the rate of heat generation. To avoid overheating, the components have to be thin, light, and short. At the moment, the rate of failure of electronic components rises as temperature rises, therefore, the higher the temperature increases, the lower the reliability (i.e., laptops and computers). Thermal management systems (i.e., heat sinks) need to be optimised to achieve optimal performance in the given region due to the exponential growth in heat input in air cooling equipment.

Heat sinks are passive electronic devices that direct heat dissipation from a hot system and cool associated parts, thereby improving their performance, reliability, and preventing premature breakdown [1]. The heat sink is mostly constructed of high-quality thermal conducting material to remove undesired heat and obey Fourier's law of conduction [2]. Many studies focused on, heat sinks with square, circular, and honeycomb enclosures [3], airfoil-shaped pin-fins heat sinks [4], foam-fin heat sinks [5], twisted hexagonal fins [6], straight with add semi-circular, triangle, and square fin heat sink [7], sinusoidal wavy plate-fin heat sink [8], micro pin-fin [9], microchannel heat sinks [10], branched and interrupted fins heat sink [11], taper sloped fin heat sinks [12], tree-like sinks [13] and many other types are now being used to improve heat transfer.

The surface texture refers to the geometric irregularities found on the surface, appearing as a sequence of peaks and valleys with varying heights and distances. Surface roughness is a crucial aspect of surface texture that measures the height of peaks and valleys. Several roughness parameters are employed to describe the surface profile. Ra is the most frequently employed parameter, representing the arithmetic mean deviation of the profile being assessed. The maximum height of the profile, Rz, is a crucial surface parameter that

✉ Prveen Bidare  
p.bidare@shu.ac.uk

<sup>1</sup> Excelfast Advanced Technologies Pvt. Ltd, Indore, Madhya Pradesh 452012, India

<sup>2</sup> Manufacturing Made Easy Ltd, 47 Welby Place, Sheffield S8 9DA, England, UK

<sup>3</sup> School of Engineering and Built Environment, Sheffield Hallam University, Sheffield S1 1WB, UK

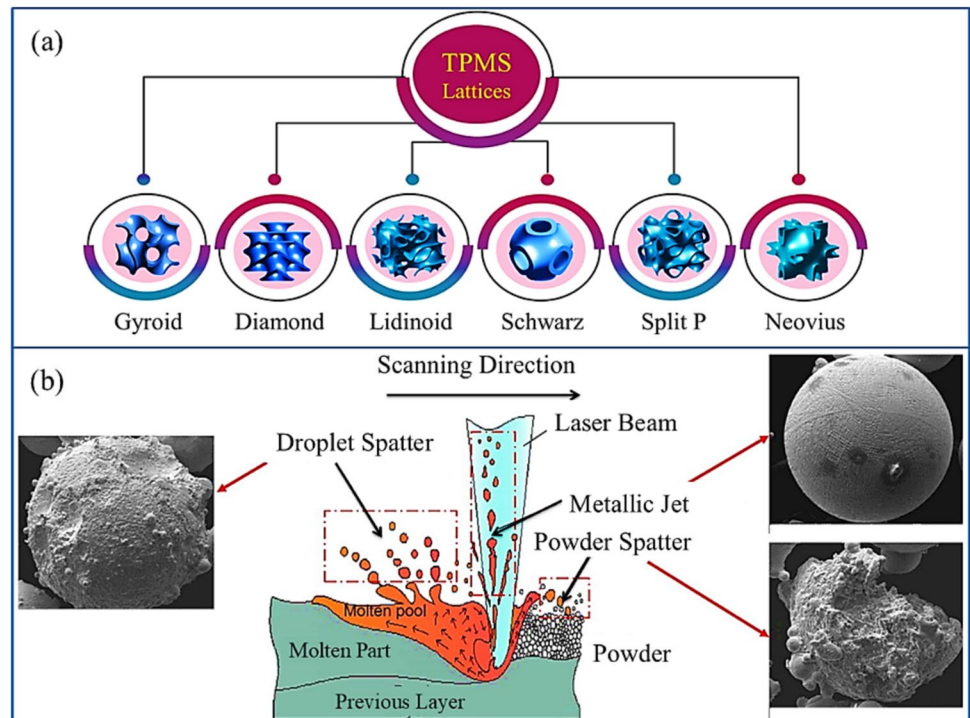
is calculated by adding the height of the tallest peak to the depth of the lowest valley. within a specific sampling length, also referred to as peak to valley. In commercial implant systems, metal parts consistently exhibit an acceptable roughness with a height variation ( $R_a$ ) ranging from 1 to 2  $\mu\text{m}$ . The roughness levels are categorized as smooth ( $R_a < 0.5 \mu\text{m}$ ), minimally rough ( $R_a 0.5\text{--}1.0 \mu\text{m}$ ), moderately rough ( $R_a 1.0\text{--}2.0 \mu\text{m}$ ), and highly rough ( $R_a > 2.0 \mu\text{m}$ ).

Typically, these roughness features are obtained via sandblasting with multiple metals or metal oxides, etching, machining, coatings of micron-sized metal beads, or anodisation. The ejection of solids or liquids from a melt zone, known as a spatter, is a typical occurrence in laser manufacturing processes. LPBF is quite a complicated process and it follows the ISO/ASTM 52900 standard [14]. A substantial amount of molten droplets and powder particles are expelled from the melt pool and often fall back into the powder bed, causing damage to the powder layers. The "spatter" phenomenon inside the build chambers of additive manufacturing system is caused by gas flow. The formation of splatter has a negative effect on component functionality. Droplet spatter occurs when molten metal is torn apart, while powder spatter is created when non-molten metallic powder particles around the molten pool are dispersed (see Fig. 1) [15]. Other factors contributing to spatter include the effects of laser power, scan speed, ambient pressure, the alloy used, and instability in the melt pool [16].

In addition, analytical approaches were used to investigate certain modern heat sink difficulties. Naga Raju

and Sivakumar [17] investigated the impact of different pin–fin designs (rectangular, circular, triangular, and interrupted rectangular) on heat sink performance and found total heat flux is higher for the Interrupted rectangular fin. Furthermore, the work from Ji et al. [18] explored the heat transfer and pressure drop performance of fractal-structured silicon-based microchannel heat sinks with bifurcation angles. The research [19] proposes a numerical and experimental work of a plate fins heat sink to optimize surface area and heat transfer during forced convection to overcome the problem of overheating. Hajjalibabaei and Saghir [20] conduct a critical review of the influencing parameters and numerous designs for straight and wavy microchannel heat sinks and utilize various nanofluids to improve heat enhancement and overall thermal performance. Righetti et al. [21] proposed an innovative solution for latent thermal energy storage (LTES) systems that integrates phase change materials (PCMs) within three distinct aluminium 3D periodic structures. Their experimental investigation revealed that the combined structure significantly enhances performance during both the charging and discharging phases. Matteo Morciano et al. [22] explored the intriguing potential of an aluminum cartesian lattice infiltrated with paraffin wax for latent thermal energy storage. Their research unveiled impressive optimization in performance during both the charging and discharging phases, showcasing how this innovative approach can significantly enhance thermal energy storage efficiency. This combination of materials not only opens new avenues

**Fig. 1** **a** Triply periodic minimal surface family structures, and **b** different types of spatters [15]



**Table 1** The level-set approximation equations surface equations are used to generate each TPMS

TPMS lattice	Level set equation $f(x,y,z)=t$
Gyroid	$\sin X \cos Y + \sin Y \cos Z + \sin Z \cos X$
Diamod	$\sin X \sin Y \sin Z + \sin X \cos Y \cos Z + \cos X \sin Y \cos Z + \cos X \cos Y \sin Z$
Lidinoid	$\sin 2X \cos X \sin + \sin 2Y \cos Z \sin + \sin 2Z \cos X \sin - \cos 2X \cos 2Y - \cos 2Y \cos 2Z - \cos 2Z \cos 2X + 0.3$
Schwarz P	$\cos X + \cos Y + \cos Z$
Split P	$1.1(\sin 2X \sin Z \cos + \sin 2Y \sin X \cos + \sin 2Z \sin Y \cos X)$ $- 0.2(\cos 2X \cos 2Y + \cos 2Y \cos 2Z + \cos 2Z \cos 2X)$ $- 0.4(\cos 2X + \cos 2Y + \cos 2Z)$

for energy management but also exemplifies the fusion of structural engineering and thermal technology.

Brazilian weevils, human retinas, butterfly wings, and other species with minimal surface structures have all been uncovered by humans during their scientific study of nature [23]. Recent research findings unequivocally demonstrate that the triply periodic minimal surfaces (TPMS) lattice structures possess exceptional strength and superior thermal output. This is primarily due to their unique architected, interconnected pore space, lightweight nature, regular repeated structure, and high surface area to volume ratio, rendering them highly suitable for heat exchangers [24]. Peng et al. [25] conducted a numerical analysis of a novel TPMS-based heat exchanger, demonstrating a 7.5-fold increase in heat transfer rates compared to a conventional plate heat exchanger. Kim and Yoo [26] used a volumetric distance fields technique to create a revolutionary TPMS-based compact heat exchanger with a variety of geometries, core structures, and entrance and exit ports. The designs support the gyroid lattice for effective heat sink/exchanger applications due to providing a higher surface area to volume ratio, resulting in higher heat transfer rates.

From the previous studies, it is evident that the TPMS lattice structure outperforms conventional heat sinks. Alketan et al. [27] designed sheet-networks gyroid, solid network gyroid, and solid diamond heat sink and concluded that sheet network gyroid exhibited the highest convective heat transfer coefficient and pressure drop. Previous research on lattice-based heat sinks has predominantly focused on designs exceeding 20–30 mm, primarily addressing fluid flow and thermal simulations. However, there remains a significant gap in research concerning compact sizes, as aspects like manufacturability and experimental testing have been largely neglected [28–32]. This study aims to fill that gap by providing a detailed examination of the compact design and manufacturability of A20X TPMS heat sinks. Our work includes an analysis of 14 periodic designs, explores the capabilities of LPBF (laser powder bed fusion) manufacturing, and conducts extensive surface characterization to assess performance and viability.

The development of high-strength aluminium alloys is a notable achievement for the aerospace, automobile, and defence industries. The incorporation of Mn, Zr, Sc, and Cu elements into Al alloys, overcoming crack formation, reducing pores generation, and improving the microstructure like fine surface grains [33]. The tensile strength and elongation of several aluminium alloys made by LPBF are poor [34]. Recently, Aluminium Materials Technologies Ltd, (Worcester, UK) collaborated with the University of Birmingham to create the aluminum-copper alloy with TiB<sub>2</sub> doping known as A20X [35, 36]. Although it is lighter than most typical casting alloys for aluminum, A20X is stronger than most of them, which attracts interest from the automotive industry today [37]. Printing complex three-dimensional (3D) metallic structures is possible using the commonly used additive manufacturing technique known as selective laser melting (SLM) [38].

This study represents a significant advancement in the design and production of compact heat sinks, achieved through the innovative application of TPMS lattice structures with two unit cell sizes and varying periodicity as a crucial geometric parameter for LPBF printed heat sinks. In order to demonstrate this innovative idea, a thorough experimental investigation was carried out using commercial A20X aluminum powder. The investigation carefully examined how lattice types, unit cell sizes, and varying periodicity could positively influence the manufacturability of lattice heat sink performance. Texture analysis by scanning electron microscopy (SEM) was conducted on the surfaces of AM-printed TPMS heat sinks to examine surface irregularities. Additionally, an optical profile meter was utilized for high-resolution 3D surface mapping.

## 2 Materials and method

### 2.1 Design and development of TPMS heat sinks

The study's primary objective is to design and develop compact TPMS-based lattice heat sinks that dissipate more heat

with maximum surface area. The presented work investigates the manufacturability of five TPMS surfaces (gyroid, diamond, lidinoid, Schwarz P, Split P) that were designed using the level-set approximation equations to define the topology of the structure (see Table 1). The idea of using a different TPMS surface for heat sink applications is new and is becoming popular due to the growing application of additive manufacturing. Figure 2 displays a total of 14 designs of TPMS lattices that have been created with two unit cell sizes 5 and 10, using nTopology implicit modeling application. Each lattice has two designs with a constant thickness of 1mm and a base thickness of 2mm. For the gyroid and diamond lattice, two cylindrical varying periodicity designs have been created with unit cells 5 and 10mm. To make a good comparison between the different shapes, a fixed volume was established of size  $15 \times 15 \times 15 \text{ mm}^3$  in which the

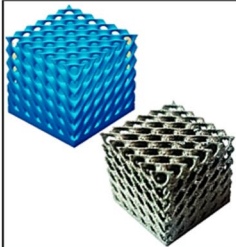
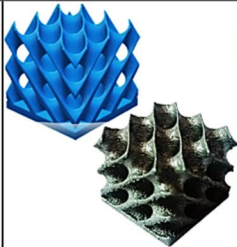
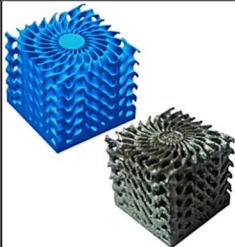
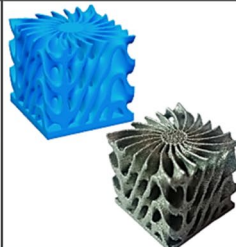

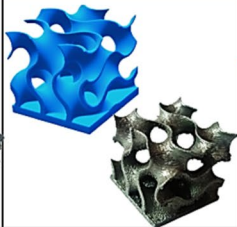
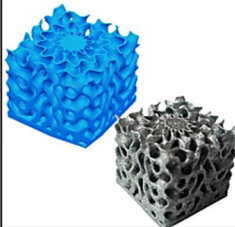
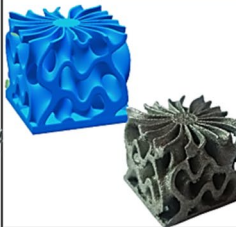
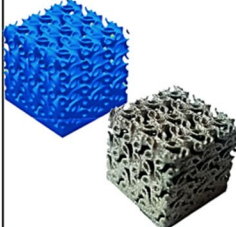
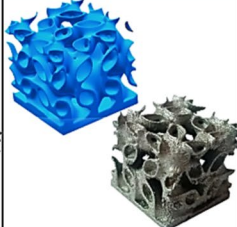
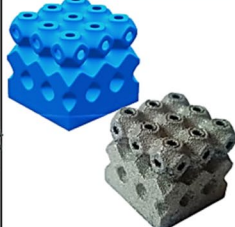
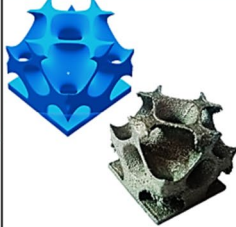
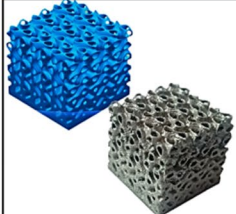

geometry must fit. In this work, a volume was defined using nTopology software to generatively design a heat sink with the maximum surface area and least amount of mass.

The TPMS equation,  $f(x, y, z)$ , is defined within cartesian space.

The spatial coordinates  $X = \omega x, Y = \omega y, Z = \omega z$ , where  $\omega$  represents are defined by  $\omega = \frac{2\pi}{l}$ , with  $l$  representing the length of the unit cell.

In this study, a comprehensive set of 14 designs for heat sinks, based on five distinct TPMS (triply periodic minimal surface) structures including gyroid, diamond, lidinoid, Schwarz P, and split P, was thoughtfully developed. These designs were then carefully converted into STL files and manufactured using selective laser melting technology to assess their manufacturability (see Fig. 2). Additive

**Fig. 2** Designs and LPBF-printed TPMS lattice heat sinks with surface area (SA). CS (cylindrical specimen) and UC (unit cell)

			
Diamond UC-5 SA- 4687.45	Diamond UC-10 SA-2821.62	Diamond CSUC-5 SA-5196.06	Diamond CSUC-10 SA-4200.04
			
Gyroid UC-5 SA-4069.36	Gyroid UC-10 SA-2395.97	Gyroid CSUC-5 SA-4771.36	Gyroid CSUC-10 SA-3625.56
			
Lidinoid UC-5 SA-5637.60	Lidinoid UC-10 SA-3789.56	Schwarz UC-5 SA-2756.60	Schwarz UC-10 SA-1981.97
	Split P UC-5 SA-5698.24		Split P UC-10 SA-3620.98

manufacturing effortlessly bridges the gap between a digital heat sink design and its physical form. The current lattice heat sinks have been produced using the concept laser M2 using laser powder-bed system situated in the School of Metallurgy and Materials at the University of Birmingham. It features a maximum build height of 300 mm and a maximum build area of 250 × 250 mm<sup>2</sup>. The M2 utilizes a continuous wave fiber laser with a variable output (up to 200 W) and a fixed focal diameter of 150 μm for scanning across the construction platform at a maximum speed of 7000 mm/s. Every build was executed in an argon atmosphere with a 20 m slice thickness (Z-increment) and oxygen content was maintained at 0.1%.

The ideal material for an additively manufactured TPMS heat sink would have excellent thermal properties for improved circulation of heat, be thin yet strong, and be suitable for the production of intricate topologies and tiny structures. The necessary material is Al-Cu alloys with TiB<sub>2</sub> doping, which meets these requirements. As the feedstock material for printing the TPMS heat sink, a spherical, gas-atomized A20X aluminium powder with a particle size range of 20–60 μm and an average particle size of 40 μm was utilized. A20X is a high-strength aluminium copper alloy that has been enhanced with titanium diboride (TiB<sub>2</sub>) doping.

**Table 2** A20x aluminium alloy material characterization and chemical composition

Material characterization		Chemical composition	
Powder morphology	Spherical	Element	Content (wt%)
Size range	20–60 μm	Cu	3.7–4.0
Average size	40 μm	Ag	0.6–1.0
Bulk hardness mean	(110.4 ± 3) HV <sub>0.1</sub>	Mg	0.3–0.6
Hardness std dev	3	Br	1.45–1.55
Average roughness	12 μm	Ti	3.49–3.71
Density (A%)	99.94	Mn	0.2–0.4
Density of the alloy	2.85 g/cm <sup>3</sup>	Si	0.10 max
		Fe	0.05 max

**Table 3** LPBF optimized process parameters for A20X alloy

Optimal parameters used for the TPMS heat sink build									
Process parameters						Laser parameters			
Parameter	Laser power (W)	Scan speed (mm/s)	Hatch spacing (μm)	Layer thickness (μm)	Energy density (J/mm <sup>3</sup> )	Beam compensation (μm)	Contour distance (μm)	Rastes type	Contour no
Value	200	1450	52.5	30	88	25	50	Island 5 × 5 mm rotated of 90° each layer	2

This unique alloy offers a strength of approximately 400 MPa while maintaining a low density, making components manufactured from A20X lightweight yet durable. It's worth noting, however, that the coefficient of thermal expansion (CTE) of aluminium-copper alloys is significantly higher than that of other materials. The summarized properties and chemical composition of these specific materials are outlined in Table 2. The expected TPMS lattice structures were effectively manufactured with interconnected unit cells, structural continuity, and high fidelity to the planned file.

Table 3 summarizes the process parameters of the AM method and laser used that are required to manufacture the heat sinks. All the TPMS heat sinks were printed with a build orientation of 90 degrees, and all measurements were taken on their side surfaces.

In Fig. 2, the surface area of all heat sinks was measured and revealed that cylindrical designs with varying periodicity significantly outshine their regular lattice counterparts. As the unit cell size increases the surface area decreases in all cases. Split P has the largest surface area in the unit cell 5 category (5698.24), whereas Schwarz's P is the lowest (2756.60). The diamond with periodicity in the unit cell 10 groups has the largest surface area (4200.04), while Schwarz P has the lowest (1981.97). Notably, the diamond lattice structure with a unit cell size of five, featuring varying periodicity, emerged as the most remarkable. Its surface area surpassed that of the standard diamond lattice with the same unit cell size by an impressive 15%. The diamond lattice structure with a unit cell size of 10, incorporating varying periodicity, exhibits a 49% increase in surface area compared to the diamond lattice structure with a uniform unit cell size of 10. In comparison with TPMS-based and conventional pin fin heat sinks (SA-2344.94 mm<sup>2</sup>), the surface area of TPMS heat sinks was nearly 1.5 times higher in the unit cell 10 groups and doubled in the unit cell 5 group.

### 3 Results and discussion

#### 3.1 Relative density measurement

To examine the impact of various TPMS surfaces and unit cell sizes on the microstructure and porosity of AM samples, the heat sinks were cut from the centre and images were captured using Hitachi TM3030 scanning electron microscopy (SEM) equipment. The images were subsequently examined with ImageJ software to determine the defect percentages in the heat sinks. Achieving near fully dense (> 99.5%) heat sinks for A20X material have been recorded. As can be seen in the Fig. 3, voids and tiny cracks have been noticed in unit cell 5 heat sink, which makes them less dense. The unit cell size 10 heat sinks demonstrate a higher density of 99.7% and unit cell size 5 shows the lowest density of 99.5%. The microstructure of the gyroid, lidinoid, and Schwarz P lattices demonstrated quite a few small spherical pores and no big pores. Small spherical pores have been found in heat sink microstructures due to the inert gas trapped in the molten metal during the LPBF process or it pre-exists in the as-received feedstock powder. The diamond and split P as-built microstructure showed some large pores. The rise in hatch spacing, scan speed, and thickness of the powder layer is responsible for the presence of these pores, which are referred to as lack-of-fusion pores.

#### 3.2 Manufacturability analysis methods

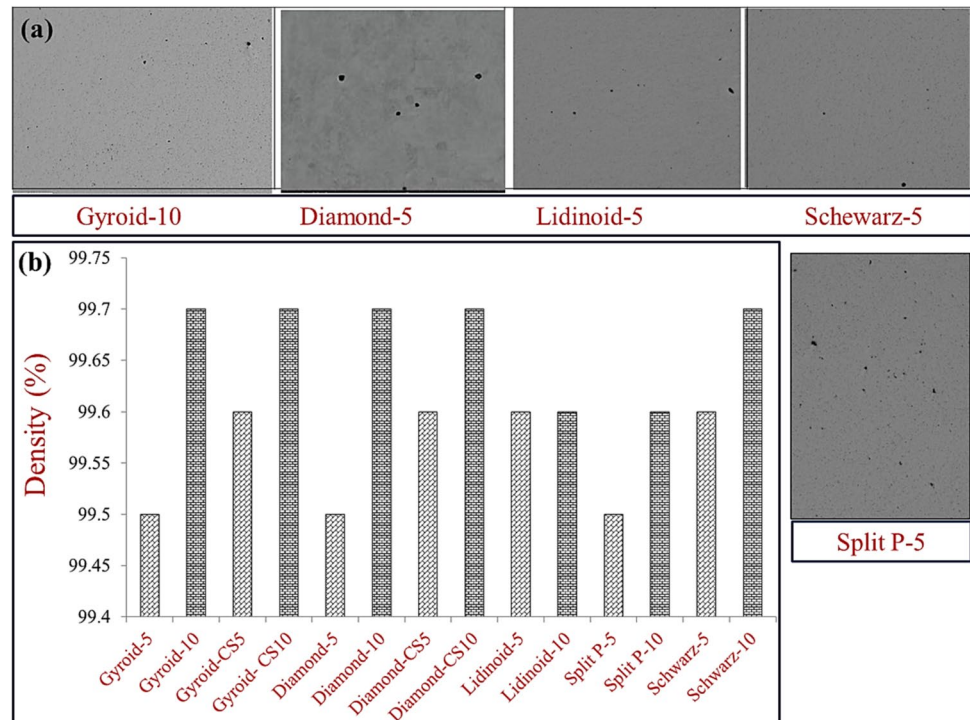
In this section, the method used to characterize the surface quality of 3D-printed lattices is described. Two principal analyses were performed: (1) surface topography, and (2) microstructural deterioration.

##### 3.2.1 Strategy on roughness

The high-resolution 3D surface topography was observed by employing the optical profile meter Alicona InfiniteFocus [IF-G4] to detect irregularities in the surface. The process involves optical scanning of the sample surface in two and three dimensions. Consequently, the measurement assesses not just profile roughness but also offers a thorough evaluation of roughness. The microscope works as a rapid non-contact optical 3D evaluation procedure that integrates the capabilities of a surface measurement system and a micro coordinate system into a single measuring device. While measuring intricate shapes and broad measurement areas of the focus instrument has a measuring range of around 3–20 mm at 400 nm and 10 nm of vertical resolution, respectively. Three measurements were taken for every round. As a result, more than 42 measurements have been taken.

Roughness parameters and types were measured for 14 LPBF additive manufactured TPMS-based heat sink samples. The means for each parameter ( $R_a$ ,  $R_q$ , and  $R_z$ ) were calculated and are displayed in Table 4. Roughness is evaluated at various spots on the outer surface of the proposed

**Fig. 3** **a** Micrographs of LPBF heat sink, and **b** relative density percentages in different TPMS heat sink

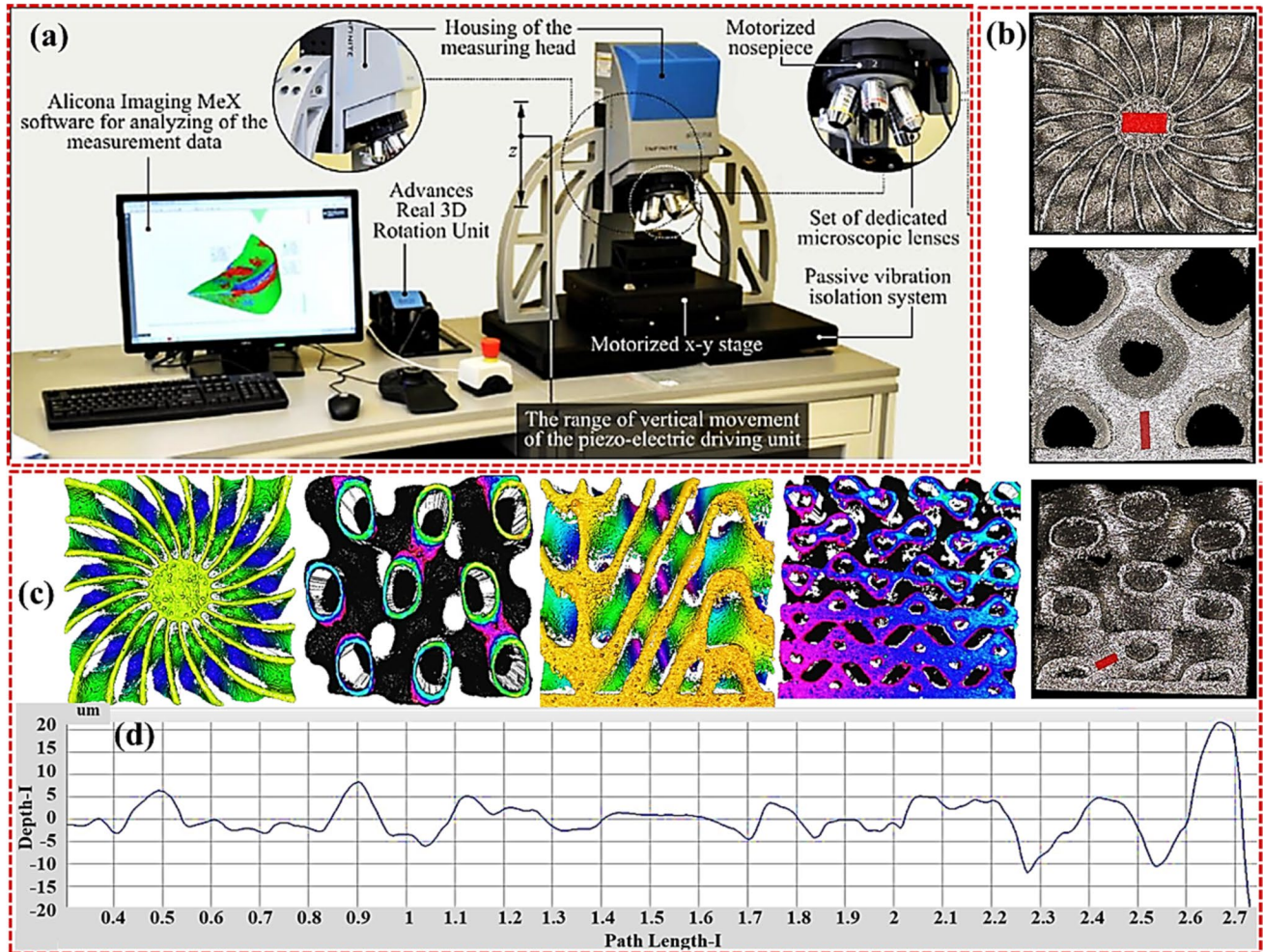


**Table 4** Evaluated roughness mean values for each heat sink and the degree of roughness

Lattice	Ra ( $\mu\text{m}$ )	Rq ( $\mu\text{m}$ )	Rz ( $\mu\text{m}$ )	Roughness type
Diamond (UC <sub>5</sub> )	2.8515	4.1930	12.5569	Highly rough
Diamond (UC <sub>10</sub> )	0.3672	0.4599	1.5452	Minimally rough
Diamond (CS-5)	3.1880	4.5761	15.1013	Highly rough
Diamond (CS-10)	3.4602	5.1532	16.7185	Highly rough
Gyroid (UC <sub>5</sub> )	2.1251	3.0245	6.5485	Highly rough
Gyroid (UC <sub>10</sub> )	1.1865	1.6079	6.1182	Moderately rough
Gyroid (CS-5)	1.6152	2.0266	7.7101	Moderately rough
Gyroid (CS-10)	1.6636	2.1792	7.7871	Moderately rough
Lidinoïd (UC <sub>5</sub> )	1.6114	1.8224	6.9127	Moderately rough
Lidinoïd (UC <sub>10</sub> )	1.4097	1.7828	6.9332	Moderately rough
Split P (UC <sub>5</sub> )	1.0311	1.3314	4.6114	Moderately rough
Split P (UC <sub>10</sub> )	1.4717	1.8634	6.1089	Moderately rough
Schwarz P (UC <sub>5</sub> )	3.2294	4.9392	18.6584	Highly rough
Schwarz P (UC <sub>10</sub> )	2.1673	2.7405	9.8828	Highly rough

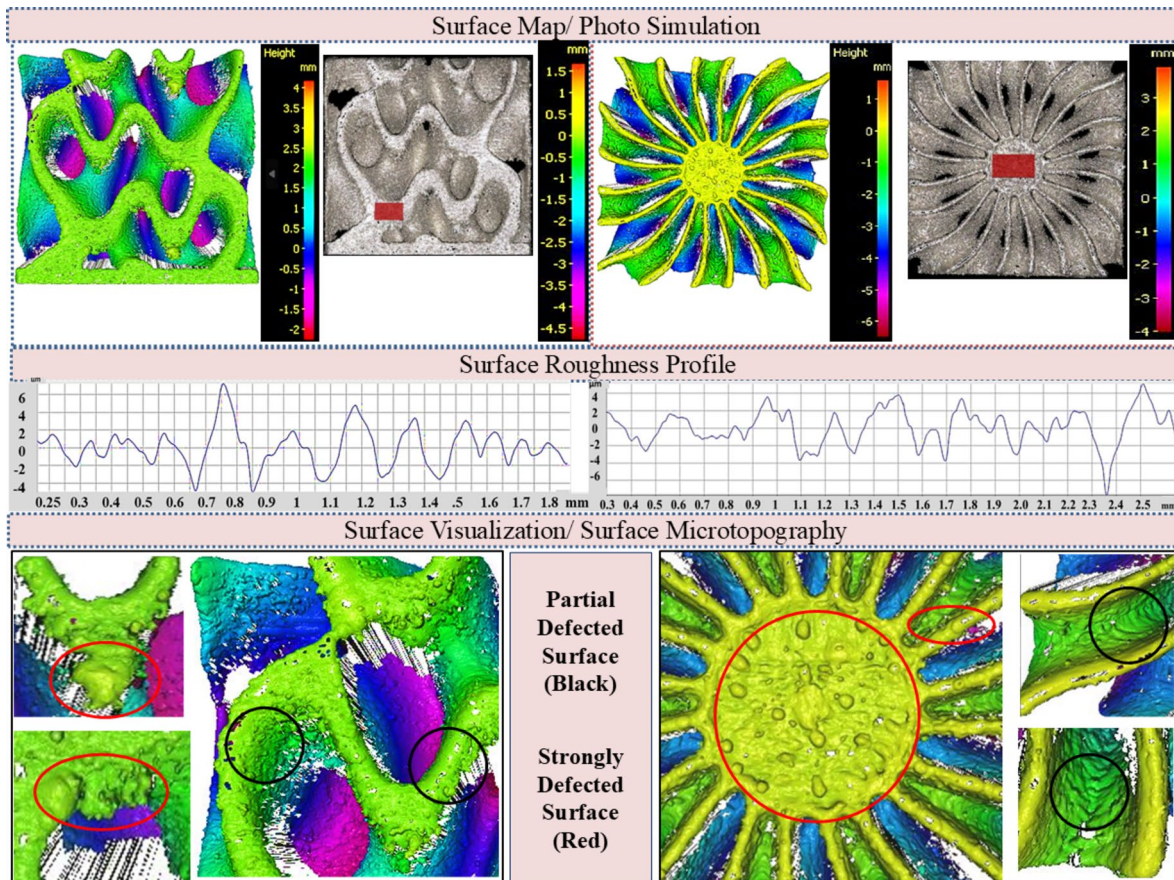
heat sinks. After assessing the roughness characteristics of a diamond lattice with a unit cell size of 10, the mean values obtained were Ra: 0.367  $\mu\text{m}$ , Rq: 0.46  $\mu\text{m}$ , and Rz: 1.5  $\mu\text{m}$ . This lattice was found to have the smoothest surface among the heat sinks. The diamond lattice design with cylindrical variable periodicity and a unit cell size of 10 showed mean roughness values of Ra: 3.46  $\mu\text{m}$ , Rq: 5.15  $\mu\text{m}$ , Rz: 16.71  $\mu\text{m}$ , indicating it has the most rough surface among heat sinks. Additionally, seven out of the fourteen heat sinks assessed were within the ideal Ra values of 1–2  $\mu\text{m}$ , indicating a fairly rough surface. The least surface heat sinks are gyroid, lidinoïd, and Split P.

Figure 4 presents the focus variation microscope Infinite-Focus [IF-G4] which is an optical non-contact profilometer with the results of surface map, surface profile, and surface microtopography of heat sinks. The surface investigation refers to the following standards: ASME B46.1-2002, ISO11562, ISO4287, and ISO4288. Focus variation and region of focus identification techniques are used in this 3D



**Fig. 4** a Optical non-contact profilometer Infinitefocus IF G4 for imaging the heat sinks samples, b printed samples, c collection of surface images, and d roughness profile





**Fig. 5** Collection of surface roughness results of gyroid heat sinks

microscope to provide a picture of height ( $z$ ) values that represent the specimen surface in true colour and as a microtopographic map. Figure 5 displays the surface map, profile, and microtopography of cylindrical varying periodicity gyroid unit cell size 10. The coordinates of the heat sink's surface can be estimated using the following coordinates:  $x = 3.119$  mm,  $y = 3.096$  mm, and  $z = 28.17$  mm and the arithmetic roughness ( $R_a$ ) is  $1.66$   $\mu\text{m}$  that is moderate and acceptable roughness. The outer walls and hanging surfaces are mainly rough. The highly rough surface in gyroid heat sinks are unit cell five sample that reflects partially melted and loose particles.

Upon the analysis of the recorded surfaces, it is clear that different types of structures have very different distributions and sizes of irregularities. Figures 6, 7, 8, and 9 show the surface profiles and roughness visualization results obtained for diamond, lidinoid, Schwarz P, and split P heat sinks. It is evident that the amount of irregularities is greater at the boundary walls and exterior hanging surfaces. These irregularities are twice as large in specific areas. According to the data provided above, the gyroid (5) surface's  $R_a$  value is approximately twice that of the gyroid (10) surface.

Whereas both circumferential gyroids have almost the same roughness values.

In Figs. 6, 7, 8, and 9, the errors are due to either the compact size of the heat sink or the degree of complexity of the lattice structure. Additionally, the material may not be evenly distributed on the build platform due to a technical process involving the machine's working arm. The distribution of irregularities, such as curved surfaces, outside walls, and inlet sections, is quite similar across the majority of the structures. However, compared to other surfaces, the surface irregularities observed in diamond UC-10 and split P UC-5 are significantly smaller.

### 3.2.2 Effect of scanning strategy on surface morphology

The second key stage of the study was to evaluate the surface morphology of the additive-manufacturing printed heat sinks. Many scientists mentioned that the laser powder bed method yields extremely complex surfaces, and melt pool instabilities frequently result in surface defects. Surface morphology was examined utilizing a Jeol JSM-6060 scanning electron microscope (SEM) equipped with an Oxford Inca energy-dispersive X-ray spectroscopy (EDX) system

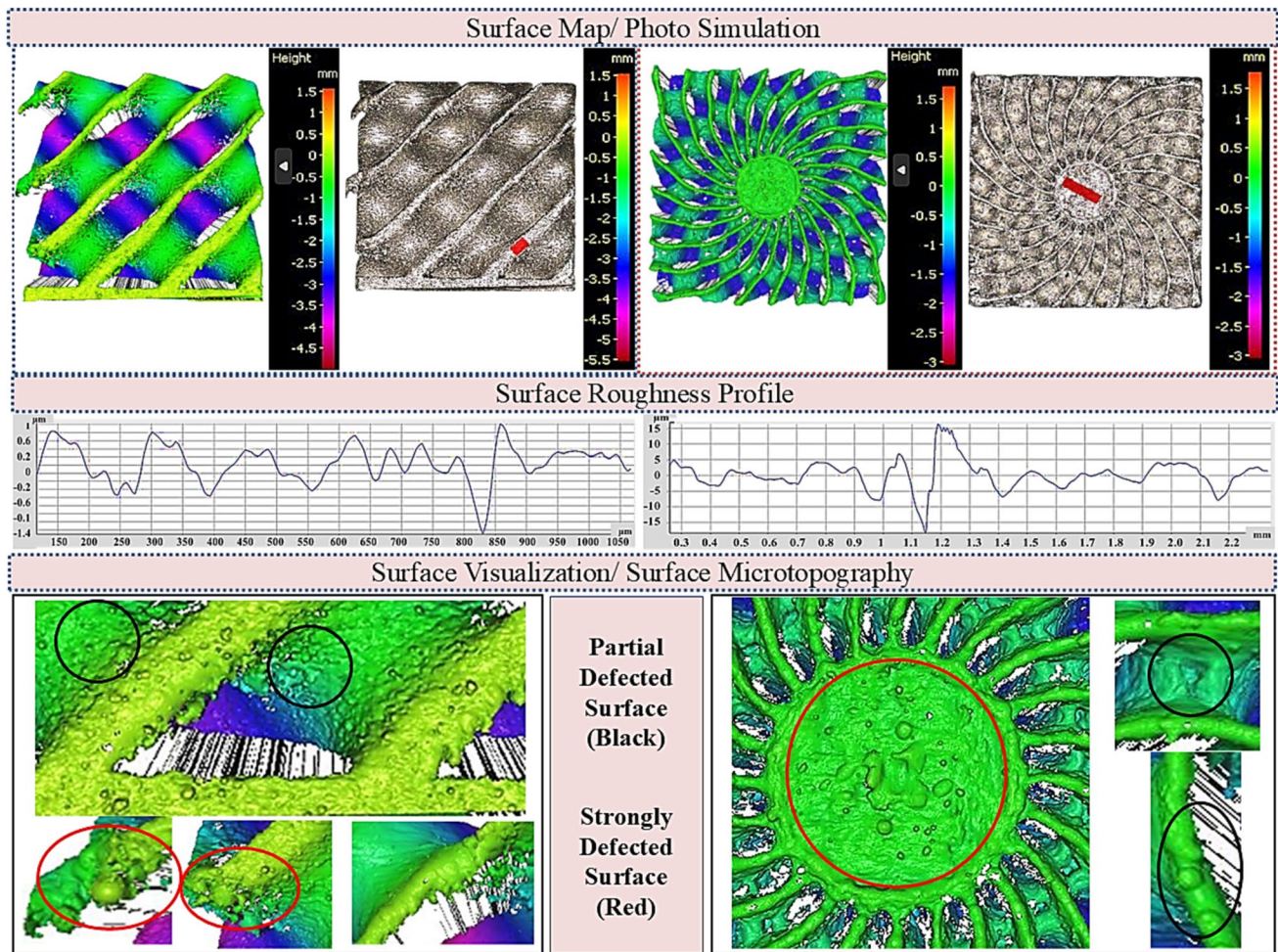


Fig. 6 Collection of surface roughness results of diamond heat sinks

under as-built conditions from all perspectives (top, front, and side). As a result of the powder-based fusion samples, common surface defects have been noticed such as the staircase effect, unmelted powder particles, adhered powder particles, powder trapped in holes, an agglomeration of powder on hanging surface, uneven layer thickness, pores, balling effect, and hot spot, which contribute to the increase of surface roughness. This kind of surface may cause a reduction in mechanical strength by acting as a stress riser. For applications like biomedical, the removal of the adhered powder particles must be achieved. In the SEM images, there are no cracks or fractured surfaces, proving that LPBF is capable of producing these TPMS cell structures.

Figure 10 displays the morphology of the diamond heat sink comprised of irregular pores and unorganized particles, which is symbolic of fusion defects resulting from insufficient heat input. The specimen contained a large number of spherical holes, which is indicative of keyhole defects. The powder was trapped in the lattice hole surface and exhibited extensive quantities of partially fused powder around the

external boundaries of the strut surface. The uneven or varying layer thickness has been noticed on top faces of diamond heat sinks,

Figure 11 illustrates the top and side faces of an LPBF-printed gyroid heat sink, which contains fewer unmelted particles than a diamond-shaped heat sink sample. The unmelted particles have been noticed on the gyroid hanging surface due to the build angle of the surface. The staircase effect appears as an outcome of layer-by-layer manufacturing, contributing to the increase in surface deviation. Uneven keyholes on the face of the gyroid heat sink were detected. The balling phenomenon and agglomeration of powder on the outer surface are responsible for to increase in mass and providing no beneficial functionality in the sample. Due to defects, Crupi et al. [39] observed the material concentration at the nodes increased by 4.1%. The balling effect varies significantly with different sizes on the top face of the heat sink. The combination of heat stresses and weak interlayer linking among particles and layers contributes to surface damage caused by the occurrence of the balling phenomenon.

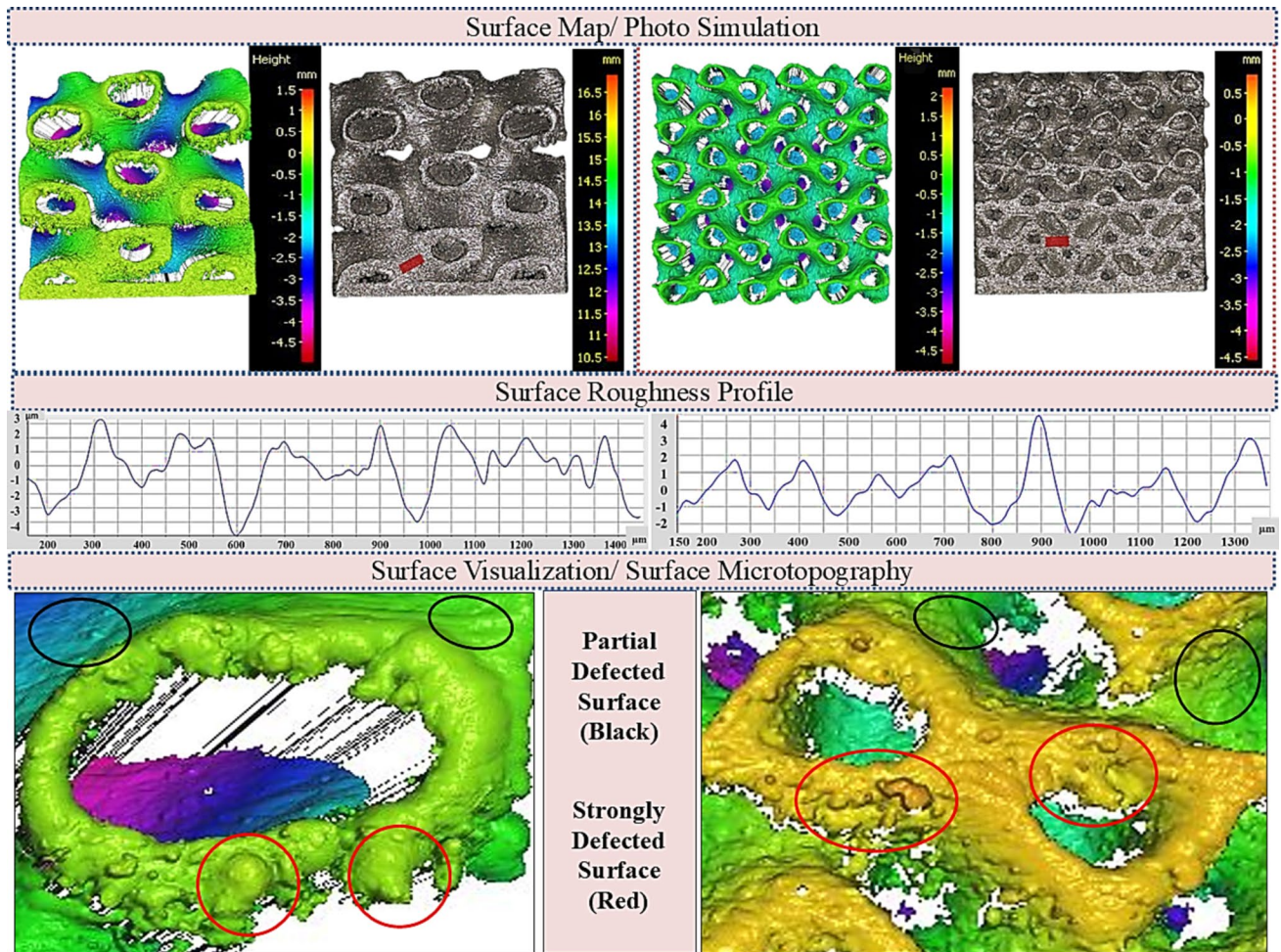


Fig. 7 Collection of surface roughness results of Split P heat sinks

The layer-by-layer terminology can be readily apparent in Fig. 12 for the lidinoid heat sink. The surface pattern of LPBF-printed TPMS heat sinks is not precisely uniform. Multiple partially melted particles are bonded to the void surface of the lidinoid heat sinks, blocking the opening channel surface. The maximum staircase effects have been observed in the lidinoid heat sink opening channel compared to other printed TPMS heat sinks. Minor pores, unmelted particles, and varying cross-sections on thickness have been noticed. Moreover, the lidinoid heat sink of unit cell 5 shows a higher rough surface compared to unit cell 10 heat sinks. Mainly higher rough surfaces have been observed at opening curve surfaces. Schwarz P unit cell is a circular geometry with six open channels, Fig. 13 presents the unmelted particles, and powder trapped in the pore section, while balling effects have been detected on the top face. An observable outcome was the presence of partially melted overhanging particles on the surface of struts. Furthermore, an increase in strut thickness compared to the design represents a typical result of lattices produced by LPBF.

Figure 14 depicts a micrograph of split P 5 and 10 unit cell heat sinks, from which it is evident that smaller unit cell heat sinks contain more surface deviation due to their smaller aperture channels. Many channels of the unit cell 5 heat sinks are almost covered with partially melted powder particles which can affect the heat transfer characteristics. split P with unit cell size 5 heat sink has the smallest unit cell and pore diameter (Fig. 14). The LPBF-printed split P heat sinks were arrested with irregularities like dimensional inaccuracy, hot shot, partially melted powder, voids, and stair-case effects. Although the stair-stepping effects can be minimised by reducing the layer thickness, doing so lengthens the manufacturing process and negatively affects the surface quality of LPBF products.

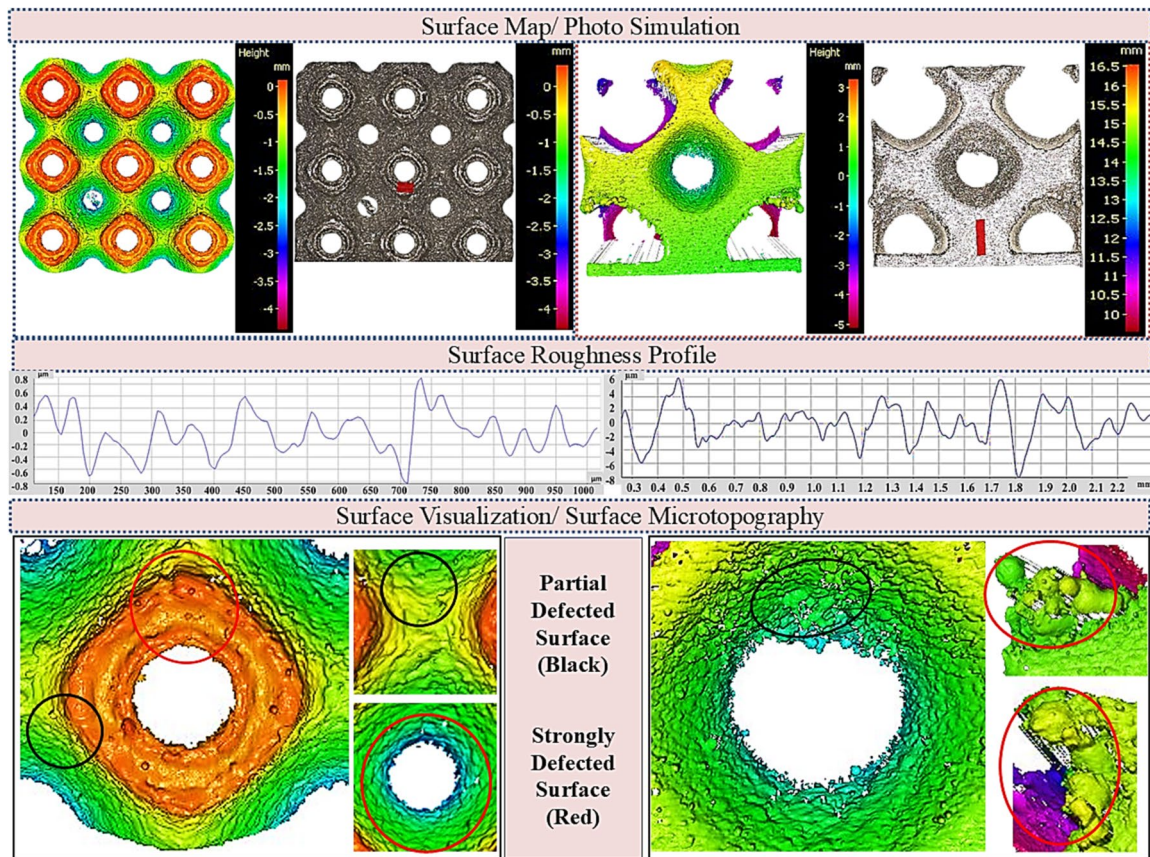


Fig. 8 Collection of surface roughness results of Schwarz P heat sinks

#### 4 Conclusion and future work

In the pursuit of manufacturability, LPBF additive manufacturing was used to build compact heat sinks featuring lattice structures, specifically TPMS structures. This endeavor aimed to assess the manufacturability of A20X material in relation to its thermal performance capabilities. The manufacturability of the TPMS lattice, including Gyroid, Diamond, Lidinoid, Schwarz P, and Split P structures, was compared using manufacturability analysis methods such as high-resolution 3D surface topography through an optical profile meter to detect irregularities in the surface and Surface morphology using a scanning electron microscope (SEM). This research emphasizes the capacity of additive manufacturing to create intricate and space-efficient designs, which can enhance the heat dissipation in power devices. The results of the study demonstrate that in comparison to a traditional rectangular fin, the TPMS-based metallic compact heat sink can be produced with a higher relative density (> 99.5%) and surface finish through the use of the LPBF additive manufacturing technique. This allows the heat sink to dissipate more heat into its surroundings. The following conclusions are derived from this study:

- In comparison to a traditional pin fin heat sink of the same size, the TPMS-based additive manufactured heat sink offers a larger surface area, which is the primary requirement for a heat transfer device.
- Beyond this threshold, the surface of the printed TPMS heat sink with smaller unit cell size appears significantly rough compared to that of the samples with bigger unit cells.
- Following powder adhesion and post-treatment, the additively manufactured sample has a bigger heat sink volume than its intended ones.
- Common irregularities have been observed in printed compact heat sinks including, voids, partially melted particles, stair-case effects, dimensional inaccuracy and balling effects. Two significant defects that have been identified on struts and inside the holes are partially melted particles and dimensional inaccuracies.
- The optical profile meter examination of the heat sinks indicates that there are more irregularities at the external hanging surfaces and boundary walls.

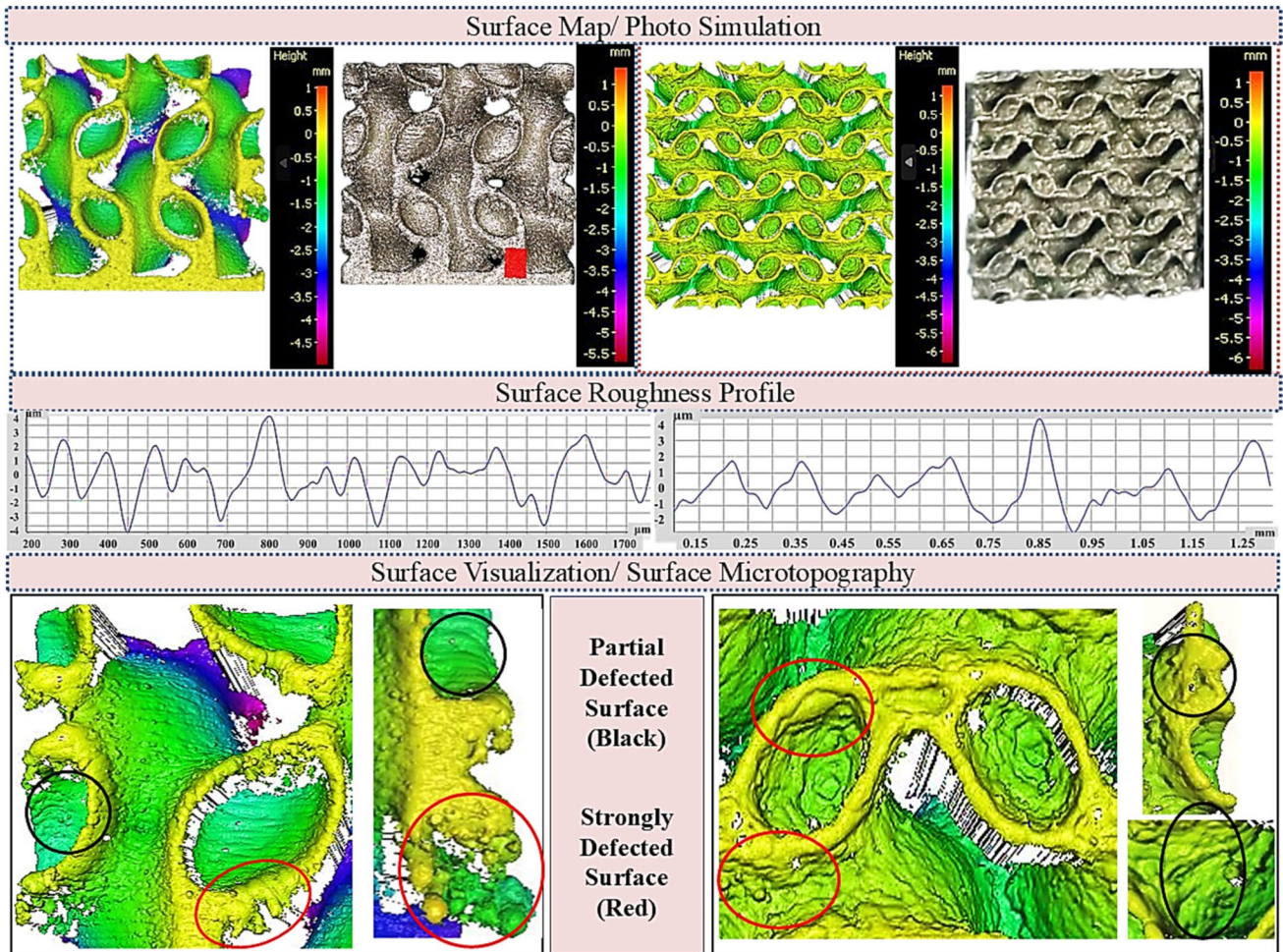


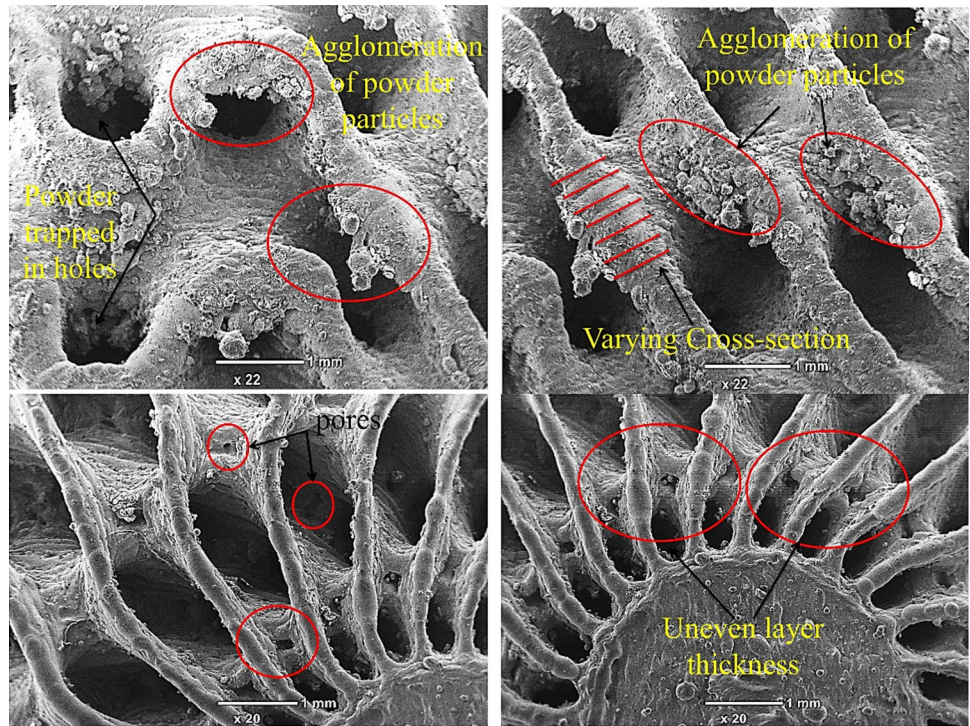
Fig. 9 Collection of surface roughness results of lidinoid heat sinks

- Conversely, in the manufacturing of complex structures, support structures are important to hold up hanging surfaces but the TPMS lattice-based structures are self-supportive in nature and due to this can be utilized as infill structures in Heat exchangers.
- The diamond lattice with a unit cell size of 10 exhibits minimal roughness, while the gyroid structure shows moderate roughness across all unit cell sizes, which is advantageous for clean printing. In contrast, the varying periodic designs of the diamond lattice in all unit cells and the Schwarz P structure in both unit cell sizes demonstrate higher levels of roughness.
- The LBPF-printed compact and intricate lattice structures characterized by small unit cell sizes represent a significant case study in achieving minimal and moderate surface roughness coupled with an increased surface area. These attributes are critical for enhancing heat transfer performance in electronic devices.

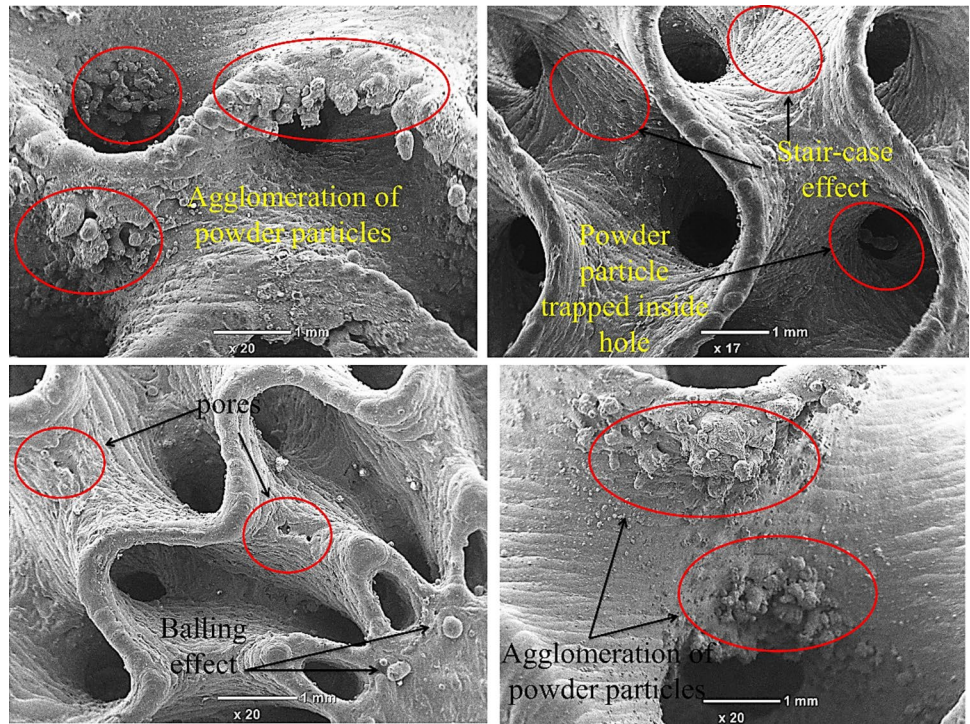
Looking forward, further research opportunities include:

The more design mappings for individual unit cells are developed, the more their manufacturability will be understood. Furthermore, the current additive manufacturing

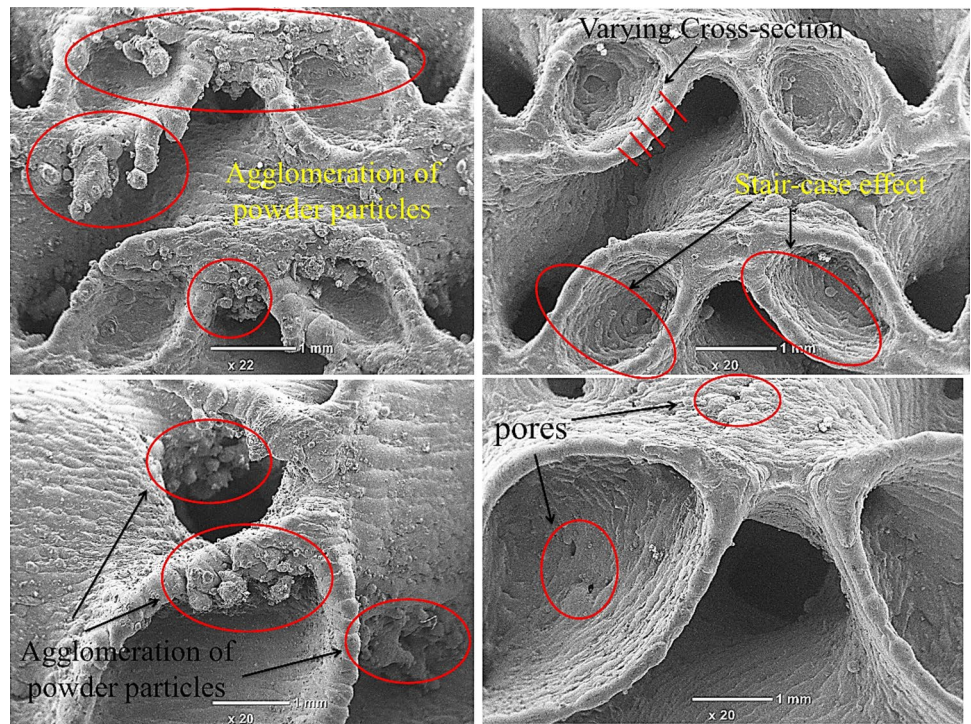
**Fig. 10** SEM results for diamond lattice heat sink top and side face



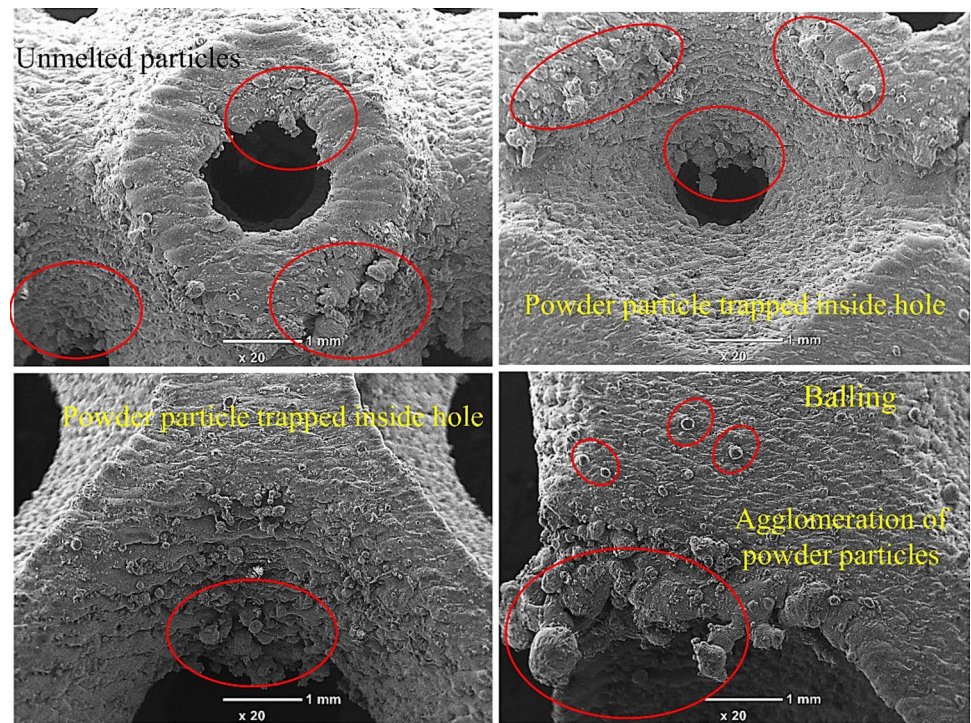
**Fig. 11** SEM image for Gyroid heat sink



**Fig. 12** SEM images of a Lidi-noid specimen



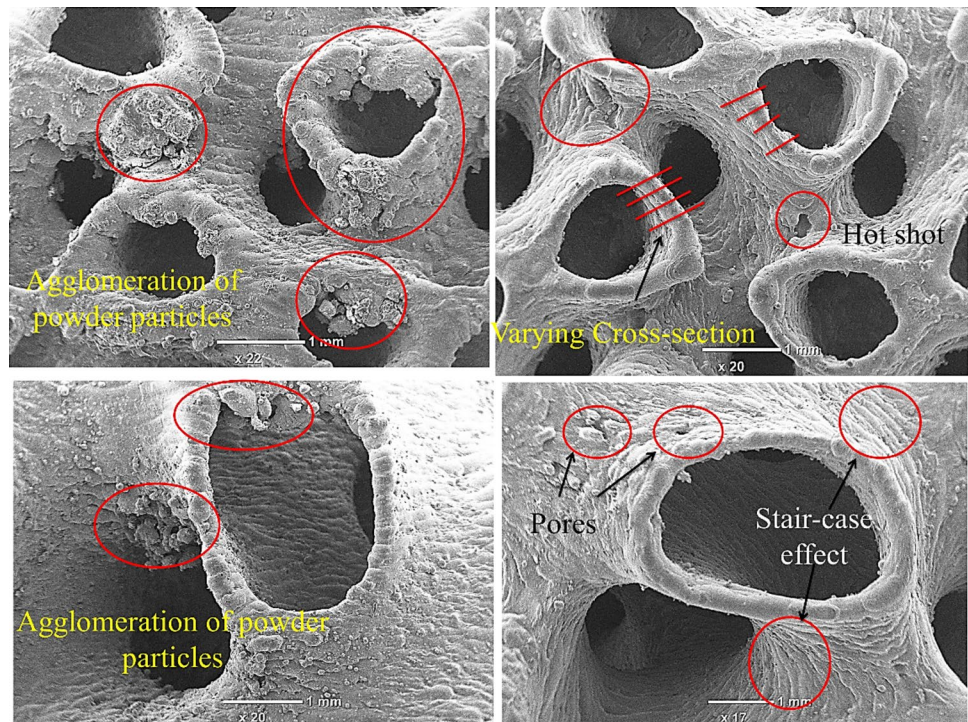
**Fig. 13** SEM images of a Schwarz P specimen



sample should be tested to check their heat transfer performance and measure how defects can affect the thermal

behaviour. Finally, this work advances the knowledge of PBF lattice structure manufacturability and speeds up the adoption of practical lattice structures across several industries.

**Fig. 14** Scanning electron microscopy micrograph of a Split P specimen



**Acknowledgements** For the purpose of open access, the author has applied a Creative Commons Attribution (CC BY) licence to any Author Accepted Manuscript version arising from this submission”

**Funding** No funding is associated with this research.

**Availability of data and materials** On request, the corresponding authors will provide all information and materials necessary to produce the findings in this study.

## Declarations

**Conflict of interest** The authors declared no conflict of interest.

**Ethical approval** The authors declare that there is no ethical issue applied to this article.

**Open Access** This article is licensed under a Creative Commons Attribution 4.0 International License, which permits use, sharing, adaptation, distribution and reproduction in any medium or format, as long as you give appropriate credit to the original author(s) and the source, provide a link to the Creative Commons licence, and indicate if changes were made. The images or other third party material in this article are included in the article’s Creative Commons licence, unless indicated otherwise in a credit line to the material. If material is not included in the article’s Creative Commons licence and your intended use is not permitted by statutory regulation or exceeds the permitted use, you will need to obtain permission directly from the copyright holder. To view a copy of this licence, visit <http://creativecommons.org/licenses/by/4.0/>.

## References

1. Chang Y-C (2020) Simulation analysis of heat transfer performance of heat sink with reduced material design. *Res Artic Adv Mech Eng*. <https://doi.org/10.1177/1687814020921300>
2. Hussein MA, Hameed VM, Dhaiban HT (2022) An implementation study on a heat sink with different fin configurations under natural convective conditions. *Case Stud Therm Eng* 30:101774. <https://doi.org/10.1016/J.CSITE.2022.101774>
3. Bhuiya R, Shah N, Arora D et al (2022) Thermal management of phase change material integrated thermoelectric cooler with different heat sink geometries. *J Energy Storage* 51:104304. <https://doi.org/10.1016/J.EST.2022.104304>
4. Babar H, Wu H, Ali HM et al (2022) Staggered oriented air-foil shaped pin-fin heat sink: investigating the efficacy of novel water based ferric oxide-silica hybrid nanofluid. *Int J Heat Mass Transf* 194:123085. <https://doi.org/10.1016/J.IJHEATMASS TRANSFER.2022.123085>
5. Samudre P, Kailas SV (2022) Thermal performance enhancement in open-pore metal foam and foam-fin heat sinks for electronics cooling. *Appl Therm Eng*. <https://doi.org/10.1016/J.APPLTHERMALENG.2021.117885>
6. Massoudi MD, Ben HMB, Almeshaal MA, Hajlaoui K (2022) Numerical evaluation of MHD SWCNT-water nanofluid performance in cooling an electronic heat sink featuring twisted hexagonal fins considering thermal emission impact: comparison between various fins shapes. *Sustain Energy Technol Assess* 53:102350. <https://doi.org/10.1016/J.SETA.2022.102350>
7. Khudhur DS, Al-Zuhairy RC, Kassim MS (2022) Thermal analysis of heat transfer with different fin geometry through straight plate-fin heat sinks. *Int J Therm Sci* 174:107443. <https://doi.org/10.1016/J.IJ THERMALSCI.2021.107443>
8. Chen Y, Chen H, Zeng H et al (2022) Structural optimization design of sinusoidal wavy plate fin heat sink with crosscut by



- Bayesian optimization. *Appl Therm Eng* 213:118755. <https://doi.org/10.1016/J.APPLTHERMALENG.2022.118755>
9. Aguirre I, González A, Castillo E (2022) Numerical study on the use of shear-thinning nanofluids in a micro pin-fin heat sink including vortex generators and changes in pin shapes. *J Taiwan Inst Chem Eng* 136:104400. <https://doi.org/10.1016/J.JTICE.2022.104400>
  10. Zhou J, Lu M, Zhao Q et al (2022) Thermal design of micro-channel heat sinks using a contour extraction based on topology optimization (CEBTO) method. *Int J Heat Mass Transf* 189:122703. <https://doi.org/10.1016/J.IJHEATMASSTRANSFER.2022.122703>
  11. Ray R, Mohanty A, Patro P, Tripathy KC (2022) Performance enhancement of heat sink with branched and interrupted fins. *Int Commun Heat Mass Transf* 133:105945. <https://doi.org/10.1016/J.ICHEATMASSTRANSFER.2022.105945>
  12. Rao AK, Somkuwar V (2022) Investigation of taper sloped fin for heat transfer enhancement in plate fin heat sink. *Mater Today Proc* 51:422–429. <https://doi.org/10.1016/J.MATPR.2021.05.567>
  13. Ho JY, See YS, Leong KC, Wong TN (2021) An experimental investigation of a PCM-based heat sink enhanced with a topology-optimized tree-like structure. *Energy Convers Manag* 245:114608. <https://doi.org/10.1016/j.enconman.2021.114608>
  14. Kusoglu IM, Gökce B, Barcikowski S (2020) Research trends in laser powder bed fusion of Al alloys within the last decade. *Addit Manuf* 36:101489. <https://doi.org/10.1016/j.addma.2020.101489>
  15. Wang D, Wu S, Fu F et al (2017) Mechanisms and characteristics of spatter generation in SLM processing and its effect on the properties. *Mater Des* 117:121–130. <https://doi.org/10.1016/j.matdes.2016.12.060>
  16. Young ZA, Guo Q, Parab ND et al (2020) Types of spatter and their features and formation mechanisms in laser powder bed fusion additive manufacturing process. *Addit Manuf* 36:101438. <https://doi.org/10.1016/j.addma.2020.101438>
  17. Raju VN, Sivakumar P, Narayana KL et al (2017) Steady state thermal analysis of heat sink with fins of different geometry. *Int J Mech Eng Technol* 8:196–206
  18. Ji X, Yang X, Zhang Y et al (2022) Experimental study of ultralow flow resistance fractal microchannel heat sinks for electronics cooling. *Int J Therm Sci* 179:107723. <https://doi.org/10.1016/J.IJTHEMALSCI.2022.107723>
  19. Altaf K, Tariq A, Ahmad SW et al (2022) Thermal and hydraulic analysis of slotted plate fins heat sinks using numerical and experimental techniques. *Case Stud Therm Eng* 35:102109. <https://doi.org/10.1016/J.CSITE.2022.102109>
  20. Hajjalibabaei M, Saghir MZ (2022) A critical review of the straight and wavy microchannel heat sink and the application in lithium-ion battery thermal management. *Int J Thermofluids* 14:100153. <https://doi.org/10.1016/J.IJFT.2022.100153>
  21. Righetti G, Savio G, Meneghello R et al (2020) Experimental study of phase change material (PCM) embedded in 3D periodic structures realized via additive manufacturing. *Int J Therm Sci* 153:106376. <https://doi.org/10.1016/j.ijthermalsci.2020.106376>
  22. Morciano M, Alberghini M, Fasano M et al (2023) 3D printed lattice metal structures for enhanced heat transfer in latent heat storage systems. *J Energy Storage* 65:107350. <https://doi.org/10.1016/j.est.2023.107350>
  23. Chouhan G, Bala Murali G (2023) Designs, advancements, and applications of three-dimensional printed gyroid structures: a review. *Proc Inst Mech Eng Part E J Process Mech Eng*. <https://doi.org/10.1177/09544089231160030>
  24. Li W, Yu G, Yu Z (2020) Bioinspired heat exchangers based on triply periodic minimal surfaces for supercritical CO<sub>2</sub> cycles. *Appl Therm Eng*. <https://doi.org/10.1016/j.applthermaleng.2020.115686>
  25. Peng H, Gao F, Hu W (2019) Design, modeling and characterization of triply periodic minimal surface heat exchangers with additive manufacturing. In: *Proceedings of 30th annual international freeform fabrication symposium—an additive manufacturing conference*, pp 2325–2337
  26. Kim J, Yoo DJ (2020) 3D printed compact heat exchangers with mathematically defined core structures. *J Comput Des Eng* 7:527–550. <https://doi.org/10.1093/JCDE/QWAA032>
  27. Al-Ketan O, Ali M, Khalil M et al (2021) Forced convection computational fluid dynamics analysis of architected and three-dimensional printable heat sinks based on triply periodic minimal surfaces. *J Therm Sci Eng Appl*. <https://doi.org/10.1115/1.4047385>
  28. Paudel BJ, Masoomi M, Thompson SM (2019) Multi-objective topology optimization of additively manufactured heat exchangers. In: *Proceedings of the 30th annual international solid freeform fabrication symposium—an additive manufacturing conference*
  29. Khalil M, Hassan Ali MI, Khan KA, Abu Al-Rub R (2022) Forced convection heat transfer in heat sinks with topologies based on triply periodic minimal surfaces. *Case Stud Therm Eng* 38:102313. <https://doi.org/10.1016/j.csite.2022.102313>
  30. Qu S, Ding J, Song X (2021) Achieving triply periodic minimal surface thin-walled structures by micro laser powder bed fusion process. *Micromachines* 12:705. <https://doi.org/10.3390/M12060705>
  31. Hassan Ali M, Alketan O, Khalil M et al (2020) 3D printed architected heat sinks cooling performance in free and forced convection environments. In: *Proceedings of the ASME 2020 heat transfer summer conference*, pp 1–7. <https://doi.org/10.1115/HT2020-9067>
  32. Baobaid N, Ali MI, Khan KA, Abu Al-Rub RK (2022) Fluid flow and heat transfer of porous TPMS architected heat sinks in free convection environment. *Case Stud Therm Eng* 33:101944. <https://doi.org/10.1016/J.CSITE.2022.101944>
  33. Sun J, Zhang B, Qu X (2021) High strength Al alloy development for laser powder bed fusion. *J Micromech Mol Phys*. <https://doi.org/10.1142/S2424913021410010>
  34. Martin JH, Yahata BD, Hundley JM et al (2017) (2017) 3D printing of high-strength aluminium alloys. *Nature* 5497672(549):365–369. <https://doi.org/10.1038/nature23894>
  35. Aluminium Materials Technologies & University of Birmingham to look deeper into A20X aluminium alloy for AM—TCT Magazine
  36. Qian L, Wang Y, Li S et al (2022) A Narrowband 3-D printed invar spherical dual-mode filter with high thermal stability for OMUXs. *IEEE Trans Microw Theory Technol* 70:2165–2173. <https://doi.org/10.1109/TMTT.2022.3152795>
  37. Qian L, Li S, Attallah M et al (2021) Thermal stability analysis of 3D printed resonators using novel materials. In: *2021 51st european microwave conference EuMC 2021*, pp 334–337. <https://doi.org/10.23919/EUMC50147.2022.9784368>
  38. Essa K, Sabouri A, Butt H et al (2018) Laser additive manufacturing of 3D meshes for optical applications. *PLoS ONE* 13:e0192389. <https://doi.org/10.1371/JOURNAL.PONE.0192389>
  39. Crupi V, Kara E, Epasto G et al (2017) Static behavior of lattice structures produced via direct metal laser sintering technology. <https://doi.org/10.1016/j.matdes.2017.09.003>

**Publisher's Note** Springer Nature remains neutral with regard to jurisdictional claims in published maps and institutional affiliations.